

Molecular dynamics simulations of dopant effectson lattice trapping of cracks in Ni matrix

Shulan Liu(刘淑兰) and Huijing Yang(杨会静)

Citation: Chin. Phys. B, 2021, 30 (**11**): 116107. DOI: 10.1088/1674-1056/ac0780
Journal homepage: http://cpb.iphy.ac.cn; http://iopscience.iop.org/cpb

What follows is a list of articles you may be interested in

Oxygen vacancies and V co-doped Co_3O_4 prepared by ion implantation boosts oxygen evolution catalysis

Bo Sun(孙博), Dong He(贺栋), Hongbo Wang(王宏博), Jiangchao Liu(刘江超), Zunjian Ke(柯尊健), Li Cheng(程莉), and Xiangheng Xiao(肖湘衡)
Chin. Phys. B, 2021, 30 (**10**): 106102. DOI: 10.1088/1674-1056/ac1339

Structural modulation and physical properties of cobalt-doped layered $La_2M_5As_3O_2$ (M= Cu, Ni) compounds

Lei Yang(杨蕾), Yan-Peng Song(宋艳鹏), Jun-Jie Wang(王俊杰), Xu Chen(陈旭), Hui-Jing Du(杜会静), and Jian-Gang Guo(郭建刚)
Chin. Phys. B, 2021, 30 (**7**): 076106. DOI: 10.1088/1674-1056/abf349

Effects of Re, Ta, and W in [110] (001) dislocation core of γ/γ' interface to Ni-based superalloys: First-principles study

Chuanxi Zhu(朱传喜), Tao Yu(于涛)
Chin. Phys. B, 2020, 29 (**9**): 096101. DOI: 10.1088/1674-1056/abad26

First-principles calculations of solute-vacancy interactions in aluminum

Sha-Sha Zhang(张莎莎), Zheng-Jun Yao(姚正军), Xiang-Shan Kong(孔祥山), Liang Chen(陈良), Jing-Yu Qin(秦敬玉)
Chin. Phys. B, 2020, 29 (**6**): 066103. DOI: 10.1088/1674-1056/ab8458

The generalized planar fault energy, ductility, and twinnability of Al and Al-*RE* (*RE*=Sc, Y, Dy, Tb, Nd) at different temperatures： A first-principles study

Wu Xiao-Zhi, Liu Li-Li, Wang Rui, Liu Qing
Chin. Phys. B, 2014, 23 (**6**): 066104. DOI: 10.1088/1674-1056/23/6/066104

Molecular dynamics simulations of dopant effects on lattice trapping of cracks in Ni matrix*

Shulan Liu(刘淑兰) and Huijing Yang(杨会静)†

School of Physical Science and Technology, Tangshan Normal University, Tangshan 063000, *China*

(Received 19 April 2021; revised manuscript received 25 May 2021; accepted manuscript online 3 June 2021)

Molecular dynamic analysis was performed on pure and doped (by Re, Ru, Co or W) Ni at 300 K using the embedded-atom-method (EAM) potentials to understand the crack formation of the doped Ni matrix in the (010)[001] orientation. When Ni was doped with Re, Ru, and W, the matrix demonstrated increased lattice trapping limits and, as a result, improved the mechanical properties. Consequently, this prevented the bond breakage at the crack tips and promoted crack healing. The average atomic and surface energy values increased when Re, Ru, and W were added. Analysis of these energy increase helped us to understand the influence these elements had on the lattice trapping limits. The fracture strength of the Ni matrix at 300 K increased because of the formation of the stronger Ni–Re, Ni–Ru, and Ni–W bonds. At the same time, doping the Ni matrix with Co did not demonstrate any strengthening effects because of the formation of Co–Ni bonds, which are weaker than the Ni–Ni bonds. Out of all dopants tested in this work, Ni doping with W showed the best results.

Keywords: alloying elements, doping, Ni crack, lattice trapping

PACS: 61.82.Bg, 62.20.mm, 62.20.mt, 82.20.Wt **DOI:** 10.1088/1674-1056/ac0780

1. Introduction

The outstanding high-temperature mechanical properties of Ni-based single crystal (SC) superalloys make them popular for applications related to advanced airplane engine blades and power-generation turbines.[1,2] The γ-Ni phase is a popular host matrix for the Ni-based SC superalloys as it affects the overall mechanical properties of the resulting materials,[2,3] while the crack in γ phase restricts its applications. Analysis of the γ phase microstructure evolution was reported[4–7] earlier. However, the fracture in superalloys are complex, and the strengthening mechanism of γ-Ni matrix is still not very clear. Thus, understandings on how to strengthen the γ-Ni matrix and minimize γ-Ni matrix fracture has been becoming the important research.

The rupture leading to a complete part failure often results from cracks, which are formed because of the atomic bond breakage. The fracture stress is closely connected to the critical activation of cracks and their propagation, which, in turn, depends on the lattice trapping of the cracks.[8] If the lattice traps the crack, it does not further propagate or heals when the mechanical loads are above or below the Griffith load ($K_{\rm th}^{\rm G}$) values, which are also called upper and lower lattice trapping limits ($K_{\rm IC}^{\pm}$), respectively. The Griffith load is defined as a material state, at which the total energy change is zero when the crack propagates in a specific lattice direction of a cell with the defined in-plane boundaries.[9] At the Griffith load, a finite lattice resistance barrier exists between the isoenergetic states, which could trap the crack tip at either state. These phenomena manifest themselves as the lattice trapping effects.

The lattice trapping of material can be affected by several factors. The lattice trapping effect depends on the kinks and the interaction range of the interatomic force field, as well as on the relative stiffness of the atomic bonds at the propagation front.[9–12] Moreover, the directions of the crack front and propagation, as well as the interatomic potential and the material's structure components, also affect the lattice trapping limit and range.[13–17] Because of the industrial importance of the Ni-based SC superalloys, understanding their brittle fracture behavior upon cracking is essential. Thus, research on crack lattice trapping of Ni matrix is needed.

Mechanical properties of Ni-based SC superalloys depend on their chemical compositions. Experiments and simulations indicated that doping superalloys with Re, Ru, Co, and W improved their mechanical properties.[18–27] Our previous work reported the lattice trapping limit increased for the Ni or Ni_3Al cracks when Re or W was added and that W incorporation yielded much stronger effects for the Ni_3Al cracks.[4,13,15] Other reports indicated the effect of Co on the crack propagation along the γ/γ' interface was minimal.[28,29] In general, Ni matrix strengthening mechanisms involving solid solution formation (with Co, Mo, W, Re, and Ru dopants) are complex. Simultaneous consideration of (i) the influence of the dopants on the mechanical properties of industrial Ni–Al–X (X = Re, Ru, Co, or W) superalloys (which was assessed pre-

*Project supported by the National Natural Science Foundation of China (Grant No. 11604237), the Natural Science Foundation of Hebei Province of China (Grant Nos. E2019105073 and E2015105079), the Scientific Research Foundation of Tangshan Normal University of China (Grant Nos. 2016A06 and 2020C03), and the Department of Education of Guangdong Province, China (Grant No. 2019GKTSCX128).

†Corresponding author. E-mail: yanghj619@126.com

© 2021 Chinese Physical Society and IOP Publishing Ltd

viously by the embedded-atom-method, EAM)[30–33] and (ii) the importance of crack lattice trapping by the Ni matrix, analysis of fracture, strengthening mechanisms, crack propagation and crack lattice trapping of the Ni matrix doped with Re, Ru, Co and/or W is needed to design the material with the best performance.

Because of the accuracy and cost concerns, experiments to obtain data for this analysis might be hard to conduct, especially at the atomic scale. However, this can be achieved by using the molecular dynamics (MD) method, a powerful and reliable approach (especially when combined with the EAM potentials) to solve the above problem and to predict the superalloy properties.[4,13,29,34–39] Re, Ru, and Co dopants predominantly accumulated in the γ phase, while W was observed in both γ and γ' phases.[40,41] Therefore, this work focused on building a model with random substitution of Ni by 1 and 3 at.% of X (X = Re, Ru, Co or W) in the γ matrix. We performed MD simulations to understand how these dopants affect Ni matrix crack lattice trapping limit and range at 300 K (the simulations showed that the Ni crack propagates in a brittle manner at 300 K). We also calculated the corresponding mechanical properties, surface energy, and atomic bonding strength of the Re, Ru, Co, or W doped γ-Ni matrix.

2. Computation details

2.1. Calculation model

We constructed a model with a sharp crack in the (010)[001] orientation (with the crack plane and crack front oriented perpendicular to the [010] and parallel to the [001] directions) according to the anisotropic linear elastic displacement field[42] (see Fig. 1(a)). The atomic configurations for the cracks in the undoped and 3 at.% doped Ni matrix are shown in Figs. 1(b)–1(d). The model contained 120, 160, and 160 atomic layers along the x, y, and z ([100], [010], and [001]) directions, respectively, which accounts for the 1536000 atoms in total. To confirm the appropriate and feasible model size, two larger models with 3 at.% Re atoms were also constructed. One of these large models expanded the side lengths in x and y directions and contained 200, 200, and 160 atomic layers along the x, y, and z axes, respectively. The other large model expanded the side length in the z-direction and contained 120, 160, and 200 atomic layers along the x, y, and z axes, respectively. The smaller-sized model adopted in this work was chosen because the configuration evolution and physical properties (such as surface energy and elastic constants) did not depend on the system size. The initial crack length was set as $1/3$ of the crack propagation length.

The boundary conditions in the z-direction during the lattice trapping calculations were periodic. For the x and $y$directions, we used the fixed-displacement boundary conditions of the six outer atomic layers. Dopant atoms (at both 1 and 3 at.% levels) substituted Ni atoms randomly. Such setup showed reliable results in previous studies.[4,13,29,34] To further confirm this setup reliability, we studied three different random distributions of Re atoms at 3 at.% doping level. The deviations of the lattice and elastic constants as well as surface energy and lattice trapping limits for these distributions were negligible, which confirms the reliability of the current random doping scheme chosen in this work.

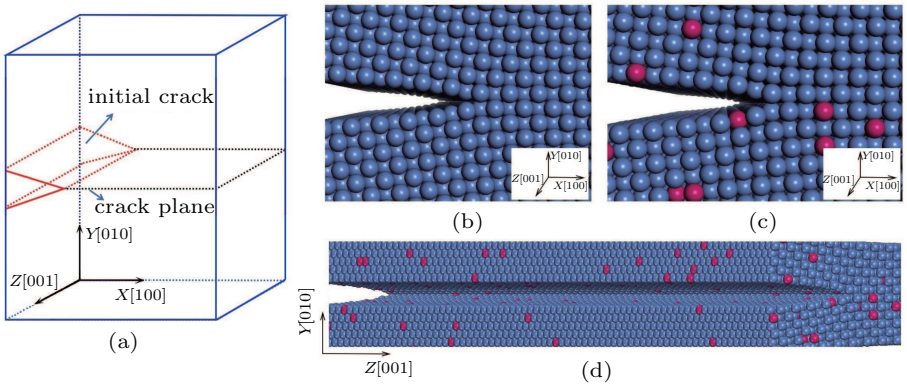


Fig. 1. A diagram showing simulation model: (a) Geometrical presentation of the lattice trapping. (b) Crack tip configuration for undoped Ni before relaxation. (c)–(d) Crack tip atomic configuration for the doped Ni (at 3 at.% level) by Re, Ru, Co or W before relaxation. Blue balls are Ni atoms; red balls are dopant atoms.

2.2. Simulation details

The Newton equations of motion at 300 K were processed by the gear algorithm[43] using 5×10^{-15} s time step. The Ni–Al–X (X = Re, Ru, Co or W) EAM potentials[30–33] of the doped matrix were used to describe the cracks. The EAM potentials were used to fit the parameters obtained from the first-principles calculations or experimental results, such as lattice constants, cohesive energies, elastic constants of Ni, Al, X (X = Re, Ru, Co or W) and their compounds. The EAM potentials typically provide reasonable results in describing the dislocations or/and crack systems of the Ni-based superalloys.[4,13,15,18,29,30,34] The

MD simulations were performed by using the XMD program.[44] During the lattice trapping modeling, the cracks were firstly simulated under different loads, after which the atoms at the crack tips were fully relaxed by using the boundary condition described in Subsection 2.1. The initial loading or unloading was set at the stress intensity to fulfill the Griffith criterion, while the crack tip was always set as stable and not allowed to advance or heal. The starting structures were in their relaxed configurations, with the further loading or unloading being proportional to the boundary displacements. The upper and lower trapping limits ($K_{\rm IC}^{\pm}$) were determined based on the sudden decrease and increase of the average bond lengths, respectively, along the crack front at the crack tip (see Fig. 2). The loading increase and decrease increments were set as 1% of the Griffith load ($K_{\rm th}^{\rm G}$). During the loading (or unloading), each relaxed step was set as 4000 for each time, while the number of the loadings (or unloadings) was 20 times of that. Thus, the total number of steps was equal to 80000. The formula for the lattice trapping range (ΔK), shown below, was taken from elsewhere:[4,13–15]

$$\Delta K = K_{\rm IC}^{+}/K_{\rm IC}^{-} - 1. \tag{1}$$

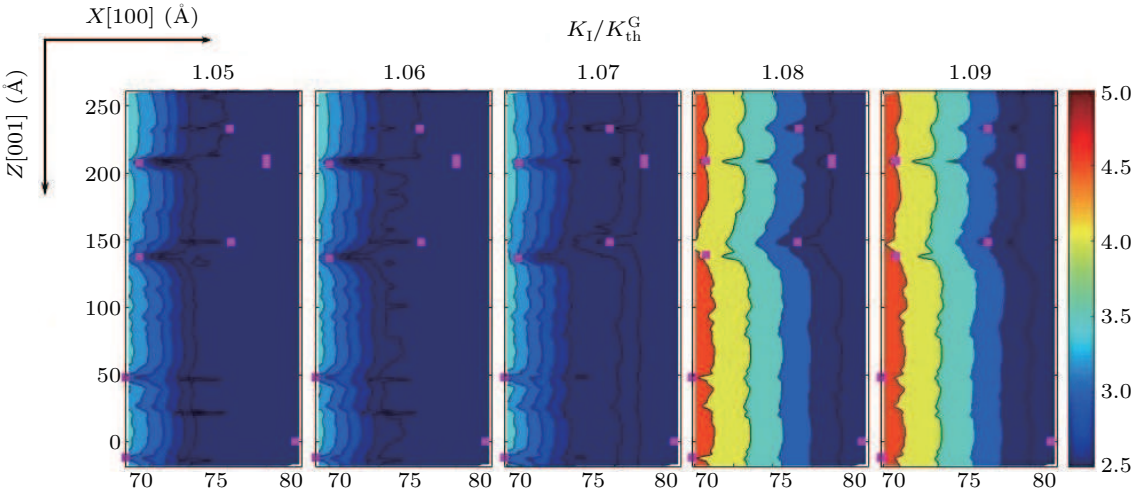


Fig. 2. An example of the bond length contour maps of atom pairs across the crack surface at the crack tip. This specific model was constructed for the 1 at.% Re-doped Ni system during the loading process. Pink squares denote the Re atom positions. The bond length bar is shown on the right-hand side.

3. Results and discussion

3.1. Mechanical parameters

To examine the reliability of the EAM potentials, the lattice constant a, the elastic constants C_{ij} (including C_{11}, C_{12}, and C_{44}), the elastic modulus (including the bulk modulus $B=(C_{11}+2C_{12})/3$, Young's modulus $E=9GB/(G+3B)$ and the shear modulus G) for the undoped and doped (at both 1 and 3 at.% levels) Ni matrix without cracks were calculated. The shear modulus G was computed as the arithmetic Hill average of Voigt ($G_{\rm V}$) and Reuss ($G_{\rm R}$) bounds as follows:

$$G_{\rm V} = \frac{1}{5}(C_{11} - C_{12} + 3C_{44}), \tag{2}$$

$$G_{\rm R} = \frac{5}{4S_{11} - 4S_{12} + 3S_{44}}, \tag{3}$$

$$G = \frac{1}{2}\left(G_{\rm V} + G_{\rm R}\right), \tag{4}$$

where S_{11}, S_{12}, and S_{44} are the elastic compliances.[45]

All calculated mechanical parameters are listed in Table 1. The value of a of the Ni matrix increased as it was doped with Re, Ru or W. However, the lattice constant of the Co-doped Ni barely changed, which agrees with the previous work.[29] The lattice parameter change upon doping can be explained by the size of the atomic radii of the dopants (which are equal to 1.37, 1.34, 1.25, and 1.39 Å for Re, Ru, Co and W, respectively) relative to the atomic radius of the matrix Ni atoms (equal 1.25 Å as well as by the interatomic interactions (discussed in Subsection 3.3). The strength of the Re-, Ru- and W-doped Ni matrix was significantly higher at the 3 at.% doping level (than at the 1 at.% level), judging by the higher values of the elastic constants C_{11}, C_{12}, and C_{44} and the elastic moduli B, E and G (see Table 1). Specifically, the values of the bulk moduli B of the Re-, Ru- and W-doped Ni at the 1 (3 at.%) level were equal to 180.72 (184.57), 179.51 (183.41), and 180.75 (184.94) GPa, respectively, which represents 1.08% (3.23%), 0.40 % (2.58%), and 1.10% (3.44%) increase in comparison to the undoped Ni matrix. The order of the matrix strengthening by the dopant addition can be described as W > Re > Ru. No difference was observed between the values of a (or C_{ij}) of the undoped Ni matrix calculated using different Ni–Al–X (X = Re, Ru, Co or W) EAM potentials, which agrees with the elastic constant values calculated previously.[29,46,47] Thus, the application of ternary Ni–Al–X (X = Re, Ru, Co or W) EAM potentials to the doped and undoped Ni matrix is a valid and reliable approach.

Table 1. Lattice (a) and elastic (C_{ij}) constants as well as bulk (B), shear (G), and Young's (E) moduli for the Ni matrix doped with 1 and 3 at.% of Re, Ru, Co or W.

Crack system	a (Å)	C_{11} (GPa)	C_{12} (GPa)	C_{44} (GPa)	B (GPa)	G (GPa)	E (GPa)
Ni-this work	3.5200	237.30	149.54	126.94	178.79	82.98	215.59
Ni-EAM[a]	3.52	241	151	127			
Ni-Exp[b]	3.52	246	147	125			
Ni-1 at.% Re	3.5237	238.91	151.62	127.86	180.72	83.17	216.32
Ni-3 at.% Re	3.5311	242.11	155.80	129.38	184.57	83.40	217.45
Ni-1 at.% Ru	3.5226	238.08	150.23	127.15	179.51	83.10	215.96
Ni-3 at.% Ru	3.5281	241.12	154.56	128.98	183.41	83.34	217.12
Ni-1 at.% Co	3.5194	235.80	148.80	126.10	177.80	82.36	214.04
Ni-3 at.% Co	3.5181	232.86	147.28	124.41	175.81	81.16	211.02
Ni-1 at.% W	3.5242	238.96	151.65	127.91	180.75	83.20	216.39
Ni-3 at.% W	3.5325	242.95	155.94	129.40	184.94	83.67	218.12

[a]Ref. [46], [b]Ref. [47].

3.2. Crack lattice trapping

3.2.1. Crack lattice trapping limits and range

The upper (K_{IC}^{+}) and lower (K_{IC}^{-}) lattice trapping limits can be determined by the jumps of the contour map of the corresponding atom pair bond lengths at the crack tip across the crack surface during the loading and unloading process.[4,13,15] As an example, the K_{IC}^{+} of the 1 at.% Re-doped Ni crack system, as well as the relationship between the K_I/K_{th}^{G} and bond length, can be seen in Fig. 2. The K_I/K_{th}^{G} range for this system was 1.05–1.09. Some bond length jumps were observed between the K_I/K_{th}^{G} values of 1.07 and 1.08 and the bond lengths evidently increased at $K_I/K_{th}^{G} > 1.07$. Thus, the value $K_{IC}^{+} = 1.07K_{th}^{G}$ corresponds to the upper lattice trapping limit for the Ni crack system containing 1 at.% of Re atoms. Therefore, this method, which checks the sudden increases or decreases of the bond lengths at crack tips (also known as "jumps"), can be used to obtain the upper and lower lattice trapping limits of doped and undoped Ni crack systems.

Figure 3 shows the lattice trapping limits and ranges ($K_{IC}^{\pm}$ and ΔK, respectively) for crack systems. K_{IC}^{+} increased as the Re, Ru or W dopants were added to the Ni matrix. When 1 at.% of Re, Ru and W atoms was incorporated, the values of K_{IC}^{+}/K_{th}^{G} (K_{IC}^{-}/K_{th}^{G}) increased by 7% (5%), 5% (4%) and 9% (8%), respectively. Thus, the addition of Re, Ru and W to the Ni matrix can prevent the crack advancement and promote crack healing. The $K_{IC}^{\pm}$ of the dopped Ni crack increased in the order of W >Re >Ru. Specifically, K_{IC}^{+} values were equal to 1.07 (1.18), 1.05 (1.15) and 1.09 (1.19) when 1 at.% (3 at.%) of Re, Ru and W were added, respectively (see Fig. 3). Thus, relative to the K_{IC}^{+} of undoped Ni matrix, the K_{IC}^{+} values for the Re-, Ru- and W-doped Ni alloy were 7% (18%), 5% (15%) and 9% (19%) higher, respectively. The addition of these dopants affected the lattice trapping limits of the Ni matrix differently. Doping with W demonstrated the strongest effect. Additionally, $K_{IC}^{\pm}$ values were higher for the 3 at.% doping levels (see Fig. 3). When Co was added, $K_{IC}^{\pm}$ decreased. Thus, Co addition would not strengthen the Ni matrix. Further elaborations on this topic will be presented in Subsection 3.3.

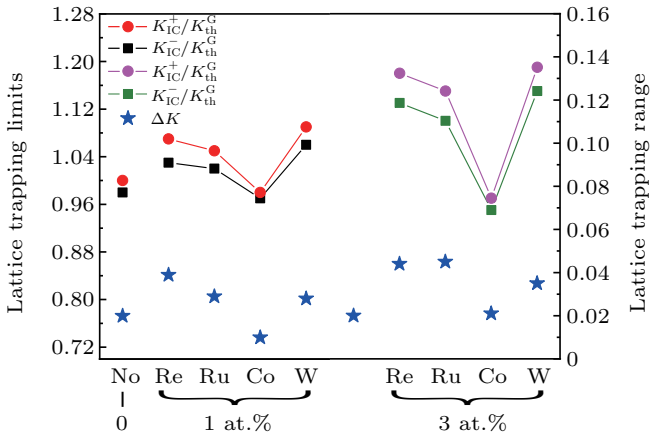


Fig. 3. Crack lattice trapping limits and ranges in undoped Ni (marked as "No") and Ni matrix doped with 1 and 3 at.% of Re, Ru, Co and W.

Our simulations showed bendings of atomic rows near the Re, Ru or W atoms were observed perpendicular to the crack propagation. Figure 4 shows the atomic configurations of the upper and lower crack surfaces under the load at the crack tip for the Ni matrix doped with 1 and 3 at.% of Re. The atomic row bendings were clearly observed near the Re atoms (shown as red balls) along the crack front. The atomic rows bendings were also observed from the contour maps of atom pairs across the crack surface at the crack tip for the Ru and W-doped Ni matrix. For example, the atom pair bond length contour maps simulated for 1 at.% Re-doped Ni under the different loads showed the atomic row bendings near the Re atoms (shown as pink squares in Fig. 2) along the crack front at $x = 71$ Å (at $K_I/K_{th}^{G} = 1.05$–1.07) and at $x = 76$ Å (at $K_I/K_{th}^{G} = 1.08$–1.09). Thus, the Ni–Re, Ni–Ru and Ni–W interactions are stronger than the Ni–Ni ones. No atomic row bendings were observed during the loading/unloading process for the crack system containing Co.

The lattice trapping ranges (ΔK) were small for all doped Ni matrices (see Fig. 3). Specifically, when 3 at.% of Re, Ru, Co or W was added, the corresponding ΔK values were equal to 0.044, 0.045, 0.022, and 0.035, respectively. Such small ΔK

values were very likely because of the long-range interatomic potential, which, according to some studies,[4,10,12,13,15,48] often indicates negligible lattice trapping by the breaking bonds. Thus, the interatomic interactions of Ni matrix doped with Re, Ru, Co or W possessed long-range characteristics.



Fig. 4. Upper and lower crack surface atomic configurations at the crack tip of Ni crack system doped with (a) 1 at.% and (b) 3 at.% of Re under loading condition. Ni and Re atoms are shown as blue and red balls, respectively.

3.2.2. Average atomic and surface energies

To further investigate the strengthening mechanisms of the doped Ni crack system, we used MD simulations to calculate the average atomic (E_{eatom}) and surface (γ) energies (see Fig. 5), defined below:[4,7,13,29]

$$E_{\text{eatom}} = E_{\text{total}}/N, \tag{5}$$

$$\gamma = \frac{1}{2}\frac{E_{\text{surface}} - E_{\text{bulk}}}{S}, \tag{6}$$

where E_{total} and N are the total energy and number of atoms in the model, respectively. EAM[30,49,50] describes the total energy as $E_{\text{total}} = \sum_i F(\rho_i) + \sum_{i>j} \varphi(r_{ij})$, where $F(\rho_i)$ is the embedding energy of atom i, $\varphi(r_{ij})$ is the two-body potential between atoms i and j, ρ_i is the host electron density at atom i contributed by the other atoms and r_{ij} is the distance between atoms i and j. In Eq. (6), E_{surface}, E_{bulk} and S are the potential energies and the area of the y plane of the systems without cracks, respectively. The "surface" and "bulk" subscripts represent the free and periodic boundary conditions along the y-direction (x and z directions were kept as periodic). The static equilibrium crack can be treated as a reversible thermodynamic system according to Griffith's theory,[51] in which the equilibrium between crack advance and new surface creation is established. The above equilibrium is given by the relation $G/2\gamma$, where $G = E_{\text{surface}} - E_{\text{bulk}}$ is the mechanical energy release upon crack advance and 2γ is the energy required for creating two new surfaces.

Small values of E_{eatom} indicate more stable systems. Figure 5 shows the calculated E_{eatom} values for each system. The addition of Re, Ru and W decreased the E_{eatom} values, which were smaller for the 3 at.% doping levels than for the 1 at.% doping levels. E_{eatom} were equal to -4.492 (-4.586) eV/atom, -4.472 (-4.528) eV/atom, and -4.502 (-4.615) eV/atom for the Ni matrix doped with 1 at.% (or 3 at.%) of Re, Ru, and W, respectively. Thus, the addition of Re, Ru, and W improved the Ni matrix stability. However, E_{eatom} did not change when Co was added to the matrix.

Surface energy γ increased as the Re, Ru, and W elements were added at the 3 at.% level (see Fig. 5). They were equal to 1626.92 J/m^2, 1621.48 J/m^2, and 1667.25 J/m^2, respectively, which is 2.22%, 1.88%, and 4.76% higher than the γ of the undoped Ni matrix (which was equal to 1591.49 J/m^2). The surface energy of the matrix did not change when Co was added. Combining this data with the average atomic and surface energies, we concluded that the influence on the strengthening could be placed in the order of W > Re > Ru > Co. The same order was obtained for the dopant effect on the lattice trapping limits discussed in Subsection 3.2.1.

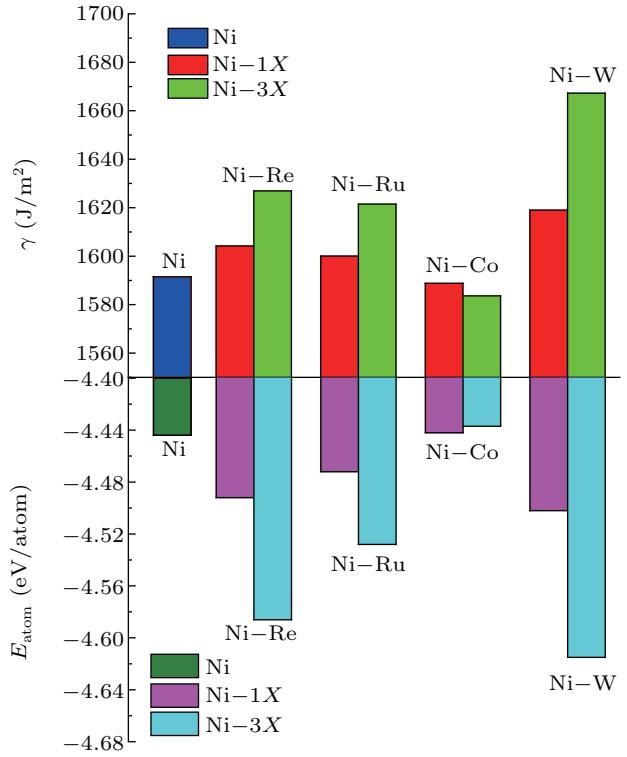


Fig. 5. The surface (γ) and the average atomic (E_{eatom}) energies for the undoped and doped (with 1 and 3 at.% of Re, Ru, Co or W) Ni crack systems.

3.2.3. Bonding strength between atoms

Earlier in this paper, we concluded that the Ni crack lattice trapping and the corresponding mechanical parameters of the Ni matrix were influenced by the dopant nature (Re, Ru, Co or W). Such behavior could be related to the interactions of the dopants with the matrix atoms. Thus, to better understand this phenomenon, we compared the strengths of the Ni–Ni, Ni–Re, Ni–Ru, Ni–Co, and Ni–W bonds by using the EAM potentials.[29,34,52]

Typically, the deeper the potential well of the EAM, the stronger the atomic bonding strength. Comparison of EAM potential wells of the Ni–Ni and Ni–X (X = Re, Ru, Co or W) bonds indicated that the Re–Ni, Ru–Ni and W–Ni interactions are stronger than the Ni–Ni ones (see Fig. 6). For instance, the absolute values of the Ni–Ni, Ni–Re, Ni–Ru, Ni–Co, and Ni–W potentials were equal to 0.21, 0.35, 0.30, 0.18, and 0.51 eV at the curve minima located at r = 2.58, 2.65, 2.61, 2.55, and 2.64 Å, respectively. Thus, the interaction strength between Ni and these dopants could be described by the order of

W > Re > Ru > Co, which agrees with the results discussed in Subsection 3.2.

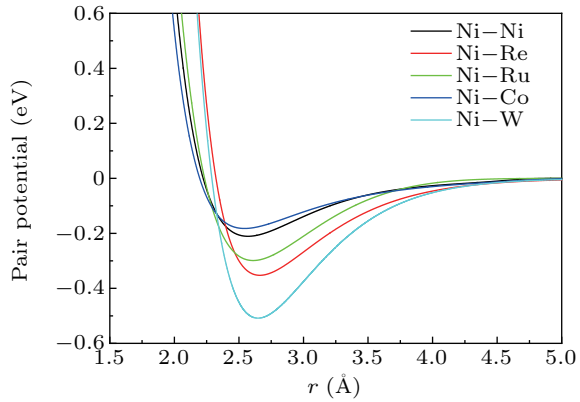


Fig. 6. Ni–Ni, Ni–Re, Ni–Ru, Ni–Co and Ni–W pair potentials calculated by EAM as a function of the atomic distance r.

The results discussed above helped us conclude that Ni doping with Re, Ru, and W created strong Ni–Re, Ni–Ru, and Ni–W bonds, which, in turn, improved the matrix mechanical properties and stability as well as prevented crack tip bond breakage and promoted the crack healing at 300 K. Doping with Co exhibited the opposite effect because of the formation of weaker Ni–Co bonds. The best Ni matrix strengthening effect and crack brittle fracture improvement were observed when 1 and 3 at.% of W were incorporated into the Ni matrix. Thus, out of the dopants tested in this work, W demonstrated the strongest effect.

4. Conclusion

This work demonstrated theoretical simulations by an MD method performed to understand how doping of Ni matrix with Re, Ru, Co, and W affect its lattice trapping at 300 K. We implemented a Ni crack model with randomly distributed Re, Ru, Co, and W, added at the 1 and 3 at.% levels. Out of all additives tested in this work, W addition into the Ni matrix demonstrated the most improved mechanical strength (namely, the elastic constants, the bulk modulus, the shear modulus and Young's modulus) and stability as well as crack advancement prevention and healing. The crack lattice trapping ranges were small for undoped and doped Ni matrices because of the long-range Ni–Re, Ni–Ru, Ni–Co, and Ni–W interatomic interactions. The comparison of the pair potential well depths obtained by EAM showed that the bonding strengths between the dopant and Ni were in the order of W > Re > Ru > Co. The Ni–Re, Ni–Ru and Ni–W bonds were stronger than the Ni–Ni ones. Out of all the dopants, W demonstrated the strongest bond with the Ni matrix, while Co exhibited the weakest.

Acknowledgement

We are grateful to Professor T. Yu and Z. G. Liu for beneficial discussions.

References

[1] Schafrik R and Sprague R 2004 *Gas Turbine Materials Adv. Mater. Process.* **162** 29
[2] Reed R C 2006 *The Superalloys* (Cambridge University Press) p. 102
[3] Pollock T M and Tin S 2006 *J. Propul. Power* **22** 361
[4] Liu Z G, Wang C Y and Yu T 2014 *Comput. Mater. Sci.* **83** 196
[5] Liu F H and Wang C Y 2017 *Chin. Phys. B* **26** 076104
[6] Qi Y, Wu W P, Chen Y B and Chen M X 2015 *RSC Adv.* **5** 65942
[7] Wang D W, Wang C Y and Yu T 2019 *R. Soc. open sci.* **6** 190441
[8] Thomson R, Hsieh C and Rana V 1971 *J. Appl. Phys.* **42** 3154
[9] Zhu T, Li J and Yip S 2006 *Proc. R. Soc. A* **462** 1741
[10] Sinclair J E 1975 *Philos. Mag.* **3** 647
[11] Schoeck G and Pichl W 1990 *Phys. Status Solidi A* **118** 109
[12] Zhang S L, Zhu T and Belytschko T 2007 *Phys. Rev. B* **76** 094114
[13] Liu S L, Wang C Y, Yu T and Liu Z G 2015 *Comput. Mater. Sci.* **97** 102
[14] Pérez R and Gumbsch P 2000 *Phys. Rev. Lett.* **84** 5347
[15] Liu S L, Wang C Y and Yu T 2015 *Comput. Mater. Sci* **110** 261
[16] Kohlhoff S, Gumbsch P and Fischmei H F 1991 *Philos. Mag. A* **64** 851
[17] Spence J C H, Huang Y M and Sankey O 1993 *Acta Metall. Mater.* **41** 2815
[18] Yue E L, Yu T, Wang Y J and Wang C Y 2021 *Intermetallics* **132** 107133
[19] Wang Y J and Wang C Y 2009 *Philos. Mag.* **89** 2935
[20] Wang Y J and Wang C Y 2009 *Appl. Phys. Lett.* **94** 261909
[21] Wang Y J and Wang C Y 2009 *Scr. Mater.* **61** 197
[22] Zhu C X and Yu T 2020 *Chin. Phys. B.* **29** 076102
[23] Reed R, Tao T and Warnken N 2009 *Acta Mater.* **57** 5898
[24] Fleischmann E, Miller M K, Affeldt E and Glatzel U 2015 *Acta Mater.* **87** 350
[25] Wang D W, Wang C Y, Yu T and Liu W Q 2020 *Chin. Phys. B* **29** 043103
[26] Ai C, Liu L, Zhang J, Guo M, Li Z, Huang T, Zhou J, Li S, Gong S and Liu G 2018 *J. Alloys Compd.* **754** 85
[27] Heckl A, Neumeier S, Cenanovic S, Göken M and Singer R F 2011 *Acta Mater.* **59** 6563
[28] Gong X F, Yang G X, Fu Y H, Xie Y Q, Zhuang J and Ning X J 2009 *Comput. Mater. Sci.* **47** 320
[29] Liu S L, Wang C Y and T Yu 2015 *RSC Adv.* **5** 52473
[30] Du J P, Wang C Y and Yu T 2013 *Modell. Simul. Mater. Sci. Eng.* **21** 015007
[31] Du J P, Wang C Y and Yu T 2014 *Chin. Phys. B* **23** 033401
[32] Fan Q N, Wang C Y, Yu T and Du J P 2015 *Physica B* **456** 283
[33] Yue E L, Yu T, Wang C Y and Du J P 2020 *Prog. Nat. Sci. Mater. Int.* **30** 539
[34] Liu Z G, Wang C Y and Yu T 2013 *Modelling Simul. Mater. Sci. Eng.* **21** 045009
[35] Zhao S J 2021 *Chin. Phys. B* **30** 056111
[36] Yu T, Xie H X and Wang C Y 2012 *Chin. Phys. B* **21** 026104
[37] Wu R H, Yin Q, Wang J P, Mao Q Z, Zhang X and Wen Z X 2021 *J. Alloys Compd.* **862** 158643
[38] Rahman M H, Mitra S, Motalab M and Bose P 2020 *RSC Adv.* **10** 31318
[39] Ye Y J, Qin L, Li J, Liu L and Wu L K 2021 *Chin. Phys. B* **30** 026801
[40] Reed R C, Yeh A C, Tin S, Babu S S and Miller M K 2004 *Scr. Mater.* **51** 327
[41] Volek A, Pyczak F, Singer R F and Mughrabi H 2005 *Scr. Mater.* **52** 141
[42] Sih G C and Liebowitz H 1968 *Mathematical Theories of Brittle Fracture, Fracture: an Advanced Treatise* (Academic Press) p. 69
[43] Allen M P and Tildesley D J 1987 *Computer Simulation of Liquids* (Oxford University Press) p. 83
[44] Rifkin J *XMD* (Center for Simulation, University of Connecticut)
[45] Grimvall G 1999 *Thermophysical Properties of Materials* (Amsterdam: North-Holland)
[46] Mishin Y 2004 *Acta Mater.* **52** 1451
[47] Simmons G and Wang H 1971 *Single Crystal Elastic Constants and Calculated Aggregate Properties* (MIT Press)
[48] Gumbsch P and Cannon R M 2000 *MRS Bull* **25** 15
[49] Daw M S and Baskes M I 1983 *Phys. Rev. Lett.* **50** 1285
[50] Daw M S and Baskes M I 1984 *Phys. Rev. B* **29** 6443
[51] Griffith A A 1921 *Phil. Trans. R. Soc. Lond. A* **221** 163
[52] Gordon P A and Neeraj T 2009 *Acta Mater.* **57** 3091